ADVANCED ELECTRONIC MATERIALS Open Access
www.advelectronicmat.de

Rapid and Ultra-Sensitive SARS-CoV-2 Subgenomic RNA Detection Using Single-Molecule With a Large Transistor-SiMoT Bioelectronic Platform

Eleonora Macchia, Anna Maria D'Erchia, Mariapia Caputo, Angelica Bianco, Claudia Leoni, Francesca Intranuovo, Cecilia Scandurra, Lucia Sarcina, Cinzia Di Franco, Paolo Bollella, Gaetano Scamarcio, Luisa Torsi,* and Graziano Pesole*

The replication of Coronaviridae viruses depends on the synthesis of structural proteins expressed through the discontinuous transcription of subgenomic RNAs (sgRNAs). Thus, detecting sgRNAs, which reflect active viral replication, provides valuable insights into infection status. Current diagnostic methods, such as PCR-based assays, often involve high costs, complex equipment, and reliance on highly trained personnel. Additionally, their specificity can be compromised by technical limitations in kit design. While viral culture remains highly accurate, it is impractical for routine diagnostics. In this study, the single-molecule-with-a-large-transistor (SiMoT) technology is presented for detecting sgRNA encoding the nucleocapsid (N) protein in clinical samples. SiMoT incorporates a stable layer of complementary DNA strands on the sensing gate electrode, facilitating rapid, sensitive, and specific sgRNA detection. Among 90 tested samples, SiMoT achieved a diagnostic sensitivity of 98.0% and a specificity of 87.8%, delivering results within 30 min. This user-friendly platform requires minimal sample preparation and offers a cost-effective point-of-care (POC) diagnostic solution. With its demonstrated diagnostic accuracy and scalability, SiMoT represents a promising tool for detecting active viral replication in SARS-CoV-2 and other coronaviruses. It addresses the limitations of existing molecular and culture-based methods while enhancing accessibility to reliable diagnostics.

1. Introduction

Coronaviridae viruses are responsible for a range of respiratory and gastrointestinal diseases, from mild to life-threatening infections.[1] These viruses possess the largest known RNA genomes, measuring between 26 and 32 kb.[2] Their RNA synthesis process consists of two main stages: genomic RNA (gRNA) replication and subgenomic RNA (sgRNA) transcription. Genome replication ensures continuous RNA synthesis, while sgRNA transcription involves a discontinuous process typical of RNA viruses, resulting in a nested set of sgRNAs. These sgRNAs encode proteins essential for viral capsid assembly, such as nucleocapsid (N), spike (S), membrane (M), and envelope (E), along with eight other proteins, some of which vary across different coronaviruses.[3] The transcription of sgRNAs in infected cells leads to the production of structural viral proteins

E. Macchia, M. Caputo, F. Intranuovo
Dipartimento di Farmacia-Scienze del Farmaco
Università degli Studi di Bari "Aldo Moro"
Bari 70125, Italy

E. Macchia
Faculty of Science and Engineering
Åbo Akademi University
Turku 20500, Finland

A. M. D'Erchia, G. Pesole
Department of Biosciences
Biotechnology and Environment
University of Bari Aldo Moro
Via Orabona 4, Bari 70126, Italy
E-mail: annamaria.derchia@uniba.it

A. Bianco
Istituto Zooprofilattico Sperimentale della Puglia e Basilicata
Putignano, Italy

C. Leoni
Institute of Biomembranes
Bioenergetics and Molecular Biotechnologies
National Research Council
Via Amendola 122/O, Bari 70126, Italy

C. Scandurra, L. Sarcina, P. Bollella, L. Torsi
Dipartimento di Chimica and Centre for Colloid and Surface Science
Università degli Studi di Bari Aldo Moro
Bari 20125, Italy
E-mail: luisa.torsi@uniba.it

The ORCID identification number(s) for the author(s) of this article can be found under https://doi.org/10.1002/aelm.202400908

© 2025 The Author(s). Advanced Electronic Materials published by Wiley-VCH GmbH. This is an open access article under the terms of the Creative Commons Attribution License, which permits use, distribution and reproduction in any medium, provided the original work is properly cited.

DOI: 10.1002/aelm.202400908

that assemble into virion particles. Detecting these sgRNAs can therefore serve as an indicator of active viral replication, instead of merely the presence of residual viral RNA.[3,4] Currently, RNA virus detection mainly depends on molecular methods like Reverse Transcription quantitative Polymerase Chain Reaction (RT-qPCR), which use primers and probes targeting the essential coding regions of viral RNA. However, this approach cannot distinguish between non-infectious residual virions and actively replicating virus particles, as it detects all viral RNA, including genomic, subgenomic, and degradation products.[5–7] For this reason, obtained results may not accurately reflect the duration of viral shedding or the transmission potential of the virus. In contrast, viral isolation and culture offer a more direct method for assessing viral replication, but this approach is complex, labor-intensive, and requires biosafety level III laboratories.[8] Due to these challenges, viral culture is not a practical option for routine clinical diagnosis of viable viral infections. Additionally, the detection of sgRNA could be pivotal in human viral challenge studies, where volunteers are intentionally infected with a challenge agent to examine both the impact of infection and the efficacy of experimental interventions, such as vaccines.[9,10] In this context, assays targeting total RNA would detect both the input challenge agent and newly replicating virus, without differentiating between them. Consequently, monitoring total RNA may not provide the most accurate measure of protective efficacy.[1,11,12] A more refined approach would be to target sgRNA instead of gRNA.

Recent years have seen significant research dedicated to the development of detection methods aimed at targeting sgRNA. These methods commonly use standard technologies such as PCR based assays and virus isolation techniques.[13] While viral isolation and culture remain the most accurate methods for determining viral replication activity, they are not practical for routine clinical diagnostics.[14] Alternatively, methods for detecting nucleic acids that target sgRNA have become promising alternatives for evaluating viral replication.[15] For example, Wölfel et al. and Oranger et al. developed specific primer/probe sets for the detection of E sgRNA, employing this approach to differentiate between actively replicating virus and viral RNA load.[3,16] Nonetheless, various studies have compared PCR-based sgRNA detection in clinical samples with viral culture results, which are considered the ultimate standard for evaluating active viral replication.[15] Furthermore, PCR-based methods face significant limitations, especially in low-resource laboratories, due to high costs, the need for complex equipment, and reliance on highly trained personnel. Additionally, some studies have reported that PCR has reduced specificity and can be affected by sample contaminants and interfering substances.[17,18] These primary limitations are often linked to technical shortcomings in PCR kit design, which may involve reagent instability, suboptimal oligonucleotide design for primers or probes, and the presence of impurities. Meanwhile, other molecular diagnostic methods, such as those based on Loop-mediated isothermal amplification (LAMP) and CRISPR-based testing, are advancing rapidly.[7] However, many of these diagnostic approaches have yet to receive global healthcare authority approvals or undergo independent validation. The single-molecule-with-a-large-transistor (SiMoT) technology is proposed here for the first time for detecting sgRNA encoding the nucleocapsid (N) protein (N sgRNA) in clinical samples. This technology has been shown to detect single proteins and genetic markers (DNA or RNA) with minimal sample handling and an assay time-to-result within 1 h, achieving a technology readiness level of 5.[19–21] The SiMoT platform has demonstrated the ability to classify and identify individual viruses in samples as small as 100 µL. Utilizing an immunometric approach, it detects the spike protein S1 on the SARS-CoV-2 capsid in blood serum, saliva, and swab samples.[20] Its diagnostic specificity, sensitivity, and overall accuracy reached 99.2%, based on 240 tests, including a pilot clinical trial.

The SiMoT platform now targets N sgRNA by using a stable layer of complementary DNA strands anchored to the sensing gate electrode. In testing a cohort comprising 90 samples, the platform has shown a diagnostic sensitivity of 98.0% and specificity of 87.8%. The SiMoT assay is also highly user-friendly, requiring only a few simple steps and delivering results in 30 min. These advantages make the SiMoT technology especially suited for point-of-care (POC) testing, providing a cost-effective, reliable, and fast method for identifying sgRNAs. **Table 1** presents a comparison of the SiMoT assay for N sgRNA detection with the leading sensor technologies and platforms. Key performance metrics are highlighted, including time-to-results, limit of detection (LOD), diagnostic sensitivity, specificity, point-of-care (POC) applicability, and labeling requirements. As a result, the SiMoT platform represents a valuable diagnostic tool for detecting active viral replication and holds promise for identifying other emerging coronaviruses in the future.

2. Results and Discussion

2.1. Surface Plasmon Resonance Characterization

Detection of the N sgRNA was achieved using SiMoT technology, where the sensing gate electrode is modified with probes specifically designed to hybridize with the target sgRNA sequence. To optimize and benchmark the biofunctionalization strategy prior to validating the SiMoT assay, Surface Plasmon Resonance (SPR) was employed. **Figure 1**a schematically illustrates the gold surface modification. The latter involves the immobilization of a biotinylated single-strand oligonucleotide sequence (b-DNA), designed to anneal to the junction region between the Leader Sequence (LS) and the ORF of N sgRNA, through a neutravidin (NAV) layer. The b-DNA probe selected in this study matches the sequence of the forward primer used in the reverse transcription-qPCR assay, specifically in the leader sequence (LS) of the N coding region, extensively characterized elsewhere.[3] Specifically, the biofunctionalization protocol begins with forming a self-assembled monolayer of alkanethiol (chem-SAM) to provide a covalent anchor for the NAV layer, followed by the

C. Di Franco
CNR IFN
Bari 70126, Italy
G. Scamarcio
CNR
Istituto Nanoscienze c/o NEST
Scuola Normale Superiore
Piazza San Silvestro 12, Pisa 56127, Italy

© 2025 The Author(s). Advanced Electronic Materials published by Wiley-VCH GmbH

2199160x, 0, Downloaded from https://onlinelibrary.wiley.com/doi/10.1002/aelm.202400908 by University Degli Studi Di Bari, Wiley Online Library on [04/02/2025]. See the Terms and Conditions (https://onlinelibrary.wiley.com/terms-and-conditions) on Wiley Online Library for rules of use; OA articles are governed by the applicable Creative Commons License

Table 1. Benchmarking the SiMoT assay for N sgRNA detection. The comparison accounts for the state-of-art where real-sample analysis is demonstrated.

Technology	LOD [copies/100 µL]	Time to results	Label-free	Diagnostic sensitivity	Diagnostic specificity	POC
PCR-based testing[3,18]	12	4–6h	No	100%	65–100%	No
LAMP[22]	400	1h	No	88.8%	89.5%	Yes
CRISP-based testing[7]	675	Within 1h	No	96.7%	97%	Yes
SiMoT	*24 ± 5*	*30 min.*	*Yes*	*98.0%*	*87.8%*	*Yes*

immobilization of the b-DNA probe via biotin/NAV affinity interaction. Importantly, although the target of the SiMoT assay is a RNA molecule, a DNA probe was chosen. This selection is based on the fact that DNA probes offer greater stability compared to RNA probes, as DNA is not vulnerable to degradation by RNases, the enzymes that degrade RNA. Additionally, previous studies have demonstrated that DNA–RNA hybridization has thermodynamic stability comparable to that of DNA–DNA hybridization.[23] The biofunctionalization protocol has been assessed in situ and in real-time through SPR, as reported in Figure 1b. SPR is a surface-sensitive spectroscopic technique that allows for detecting changes in the refractive index of an ultrathin biological layer deposited on an SPR slide, approximately half a square centimeter in size, positioned within a 100 µL flow-through cell.[24–26] When the SPR laser beam (wavelength λ = 670 nm) strikes the glass/metal interface, it can couple with plasmon surface polariton (PSP) states that travel along the metal, biolayer, and electrolyte interface. This coupling generates an evanescent wave, which propagates perpendicularly to the surface, extending about 100–300 nm beyond the metal layer. At this depth, the wave interacts with the biolayer film. For plasmon resonance to occur, meaning the complete transfer of light energy to the PSP states, the wave vector of the PSP must precisely match the component of the incident light's wave vector in both

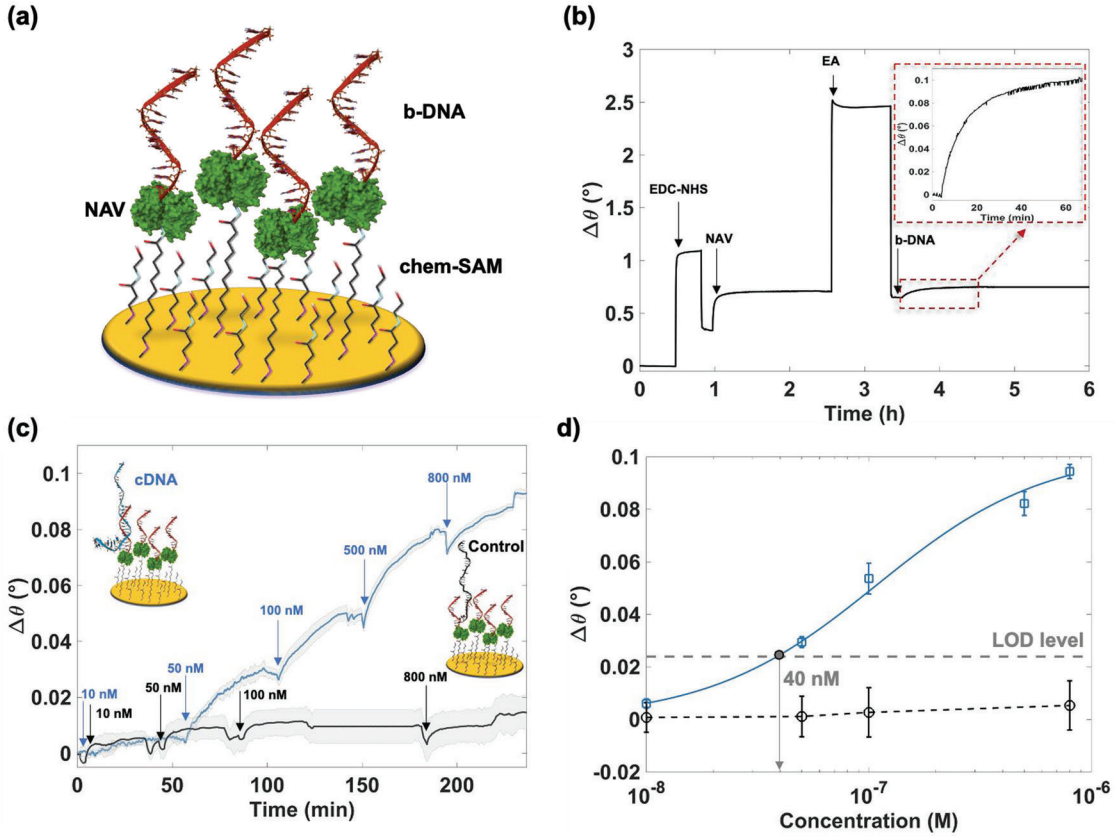

Figure 1. a) Graphical depiction of the biofunctionalized gold surface. b) SPR sensogram recorded during the biofunctionalization protocol using biotinylated DNA probes. c) Assays for standard solutions of cDNA were performed across a concentration range from 10 to 800 nM. The sensogram (blue line) represents data obtained from the biofunctionalized SPR slide exposed to varying concentrations of the target oligonucleotide, while the black line shows the sensogram from the negative control experiment, using a non-complementary strand. The grey shading indicates the standard deviation calculated from four replicate sensograms. d) Calibration curve for the cDNA assay (blue points) and the negative control experiment (black points). Error bars, representing one standard deviation from four replicates, are shown. The modeling (blue solid curve) was conducted using the Hill equation. The limit of detection (LOD), defined as the noise level (average signal from the control experiment) plus three times its standard deviation, is 40 nM.

© 2025 The Author(s). Advanced Electronic Materials published by Wiley-VCH GmbH

2199160x, 0, Downloaded from https://onlinelibrary.wiley.com/doi/10.1002/aelm.202400908 by University Degli Studi Di Bari, Wiley Online Library on [04/02/2025]. See the Terms and Conditions (https://onlinelibrary.wiley.com/terms-and-conditions) on Wiley Online Library for rules of use; OA articles are governed by the applicable Creative Commons License

magnitude and direction along the plasmonic propagation path. This match, defined by the angle θ_{SPR}, is crucial, as it enables the resonance effect and subsequent detection of refractive index changes within the thin biological layer. The SPR traces, which record the transient angle shift ($\Delta\theta_{SPR}$), are referred to as sensograms, as shown in Figure 1b. This angular shift is measured relative to the baseline signal, defined as the θ_{SPR} of the gold slide modified solely with the chem-SAM layer. The first step, illustrated in the sensogram in Figure 1b, involves the injection of an EDC/sulfo-NHS solution in water to activate the carboxylic groups of the chem-SAM.[27] Following this, a PBS solution is injected, and the activated surface is exposed to a NAV solution for 1.5 h. After rinsing with PBS, an ethanolamine (EA) solution is introduced and allowed to interact with the sensing area for 45 min, effectively blocking any unreacted activated acidic functionalities. Next, the b-DNA probe is injected and incubated on the surface for 1 h before being rinsed with PBS. As depicted in Figure 1b, the b-DNA probe is successfully immobilized on the gold sensing platform, reaching 95% of the SPR signal within 20 min. The b-DNA surface coverage is determined using the de Feijter equation,[28] which correlates the refractive index increment of the adsorbed layer with its mass density on the sensing surface. The calculated surface coverage is (52.1 ± 3.2) ng cm^{-2}, equivalent to (4.6 ± 0.2) × 10^{11} molecules cm^{-2}. Studies have demonstrated that single-stranded DNA probes immobilized on gold surfaces exhibit optimal hybridization efficiency with complementary sequences when their surface density is maintained below 5×10^{12} molecules cm^{-2}.[1,29] On the other hand, for the SiMoT platform, as extensively discussed in previous research,[24,30] it is essential to achieve a high density of biorecognition elements—on the order of at least 10^{11} molecules cm^{-2}—to ensure optimal sensitivity. This probe layer, with surface densities below the 5×10^{12} molecules cm^{-2} threshold, facilitates efficient hybridization while preserving the integrity and compactness of the capturing probe layer.

Subsequently, the modified SPR slide was exposed to a 100 bases long oligonucleotide, referred to as complementary DNA (cDNA), exclusively corresponding to the N sgRNA sequence, to assess the capability of the immobilized probe to recognize the target strand, as per Figure 1c. To establish the baseline, PBS buffer was utilized as the reference fluid. Subsequently, successive injections of 100 µL N sgRNA standard solutions were tested at increasing concentrations ranging 10 nM and 800 nM. Each concentration was incubated for 40 min, then PBS was injected as a rinsing buffer. At the highest concentration of 800 nM, the binding of the target, as shown in Figure 1c, resulted in $\Delta\theta_{SPR}$ = (0.093 ± 0.003)°, which corresponds to a surface density of (1.2 ± 0.1)·10^{11} molecules cm^{-2}. The surface density of the target strand indicates a high concentration of biomarkers deposited on the probe layer, closely corresponding to the number of probes available on the SPR slide. Those SPR analysis confirms the absence of potential allosteric interactions that could hinder the hybridization of the target strand at nanomolar concentrations. Notably, the observed SPR angle shift for the target strand aligns with the $\Delta\theta_{SPR}$ reported in previous SPR assays.[31] This consistency confirms the effectiveness of the biofunctionalization protocol developed for the SiMoT assay of N sgRNA. Figure 1c also presents the sensogram acquired during the negative control experiment, represented by a black line. This experiment was conducted to assess the assay's noise level and determine its limit of detection (LOD). For this purpose, the gold SPR sensor, functionalized with the same b-DNA probe, was exposed to a non-complementary oligonucleotide sequence of 100 bp in length, within the same concentration range as the sensing experiment. At the maximum concentration of 800 nM, a $\Delta\theta_{SPR}$ of (0.015 ± 0.006) was recorded. As a result, the assay's selectivity was calculated as the ratio of the angle shift observed in the negative control experiment to the shift measured during the sensing experiment at 800 nM, yielding a value of $\Delta\theta_{n.c.}/\Delta\theta_{s.}$ = 0.16 ± 0.01. Figure 1d displays the dose-response curves, showing $\Delta\theta_{SPR}$ as a function of nominal oligonucleotide concentrations for both the negative control experiment (black circles) and the sensing experiment (blue squares). The error bars indicate one standard deviation, calculated from four replicates. The full blue line in Figure 1d is the modeling of the dose-response curve registered for the sensing experiment, using the Hill model. The Hill model describes the relationship between the SPR signal ($\Delta\theta_{SPR}$) and the target analyte concentration (c), according to the following equation $\Delta\theta_{SPR} = \Delta\theta_{SPR,\max} \cdot \frac{c^n}{k^n + c^n}$, where $\Delta\theta_{SPR,max}$ is the SPR signal registered in the saturation. The two parameters of the model are the dissociation constant (k) and the Hill coefficient (n).[32] The Hill coefficient estimates the cooperativity of the target-probe interaction: $n = 1$ indicates non-cooperative binding, $n > 1$ suggests positive cooperativity, and $n < 1$ indicates negative cooperativity. The dissociation constant (k) represents the analyte concentration at which half of the maximum response ($\Delta\theta_{SPR,max}$) is observed or, alternatively, the concentration at which half of the binding sites are occupied. Additionally, the term k^n corresponds to the equilibrium dissociation constant (K_D) of the binding pairs, which reflects the binding affinity between the target analyte and the probe. Modeling the data in Figure 1d yielded a Hill coefficient (n) of 1.1 ± 0.2 and a K_D value of (1.1 ± 0.3) × 10^{-7}. These values align closely with Hill coefficients and dissociation constants typically observed in DNA–DNA hybridization processes,[33,34] thereby confirming the efficacy of the biofunctionalization protocol employed in this study.

2.2. SiMoT Assay of N sgRNA

The biofunctionalization protocol, developed and validated through SRP characterization, was proposed to functionalize the sensing gate of the SiMoT platform, enabling the ultrasensitive detection of N sgRNA. **Figure 2a** illustrates a graphical depiction of the SiMoT assay. The SiMoT device comprises a biofunctionalized sensing gate and a reference gate, capacitively coupled to the transistor channel. The channel includes gold drain (D) and source (S) electrodes, which are coated with a p-type organic semiconductor.[30] The sensing gate is functionalized with b-DNA probes, according to the protocol validated via SPR analysis and then exposed to the sgRNA containing solution. This exposure occurs during a 10-min incubation in an incubation well (not depicted) containing 100 µL of the solution to be tested. When the target N sgRNA sequence binds to the probes, the sensing gate's work function undergoes a significant shift.[35–37] This shift is measured through capacitive coupling with the transistor channel, resulting in a detectable change in current. To optimize the electronic sensing response, the Debye length must be

© 2025 The Author(s). Advanced Electronic Materials published by Wiley-VCH GmbH

2199160x, 0, Downloaded from https://onlinelibrary.wiley.com/doi/10.1002/aelm.202400908 by University Degli Studi Di Bari, Wiley Online Library on [04/02/2025]. See the Terms and Conditions (https://onlinelibrary.wiley.com/terms-and-conditions) on Wiley Online Library for rules of use; OA articles are governed by the applicable Creative Commons License

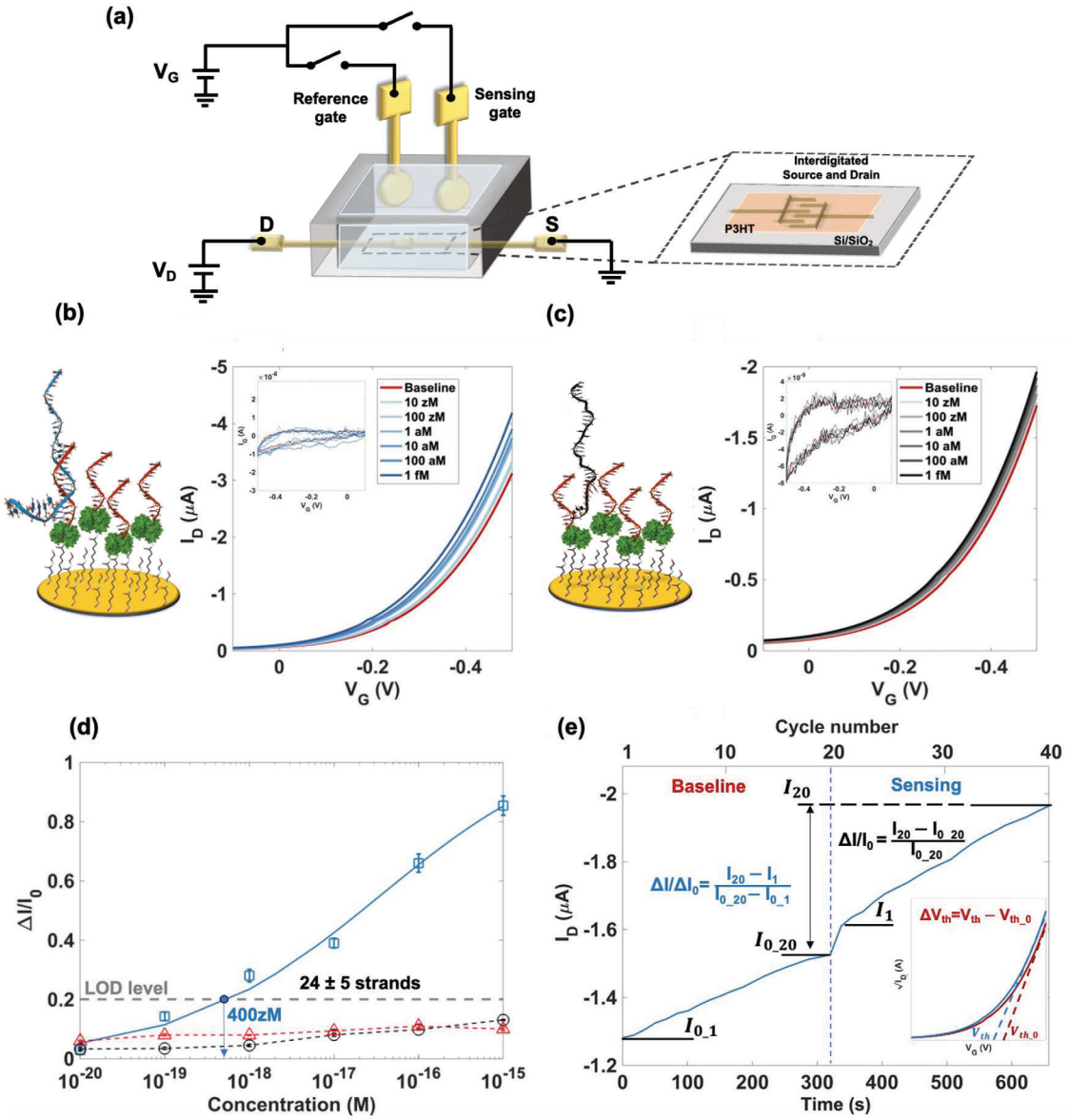

Figure 2. a) Schematic illustration of the SiMoT platform. b) Transfer characteristics (I_D versus V_G) of a typical sensing experiment and c) a negative control in forward mode, measured at $V_D = -0.4$ V with V_G swept from 0.1 to −0.5 V. The baseline current level is shown in red. The same gate was sequentially exposed to PBS solutions containing the DNA at concentrations from 10 zM to 1 fM. d) Dose-response curves displaying the relative current shift ($\Delta I/I_0$) for sensing gates (blue squares) and negative controls (black circles). Error bars represent one standard deviation across three replicates. The solid blue curve represents a 4-parameter logistic model fit. The limit of detection (LOD), calculated as the control noise level plus three standard deviations, corresponds to 24 ± 5 molecules per 100 µL. Red triangles indicate reference gate responses, remaining below the LOD. e) Time-resolved I_D measurements at $V_G = -0.4$ V, recorded before and after incubation in the sample solution.

maximized. Since the assay samples are in high-ionic-strength media (162 mM), the sensing gate is subsequently analyzed in the measuring well containing deionized (DI) water. The latter has a low ionic strength of approximately 5 µM, thus resulting in a Debye length of 138 nm.[37] However, the hybridization process occurs in a physiological medium with high ionic strength, to ensure the stability of the probe/target duplex formation. Moreover, the stability of biorecognition layers has also been demonstrated in a previous study,[26] where SPR characterization confirmed the retention of biological functionality even after extended exposure to deionized water. The reference gate, suspended stably above the channel at a distance of ≈4 mm, ensures the monitoring of the stability of the device throughout the assay. Moreover, all the incubation and measuring steps with the SiMoT assay have been accomplished under RNAse-free conditions. Figure 2b illustrates the transfer characteristics obtained during the assay of cDNA matching the sequence of the N sgRNA target using the sensing gate. These curves represent the transistor drain current (I_D) measured at a fixed drain-source voltage (V_D) of −0.4V , with the gate voltage (V_G) varied from 0.1 to −0 .5V. As described in

© 2025 The Author(s). Advanced Electronic Materials published by Wiley-VCH GmbH

2199160x, 0, Downloaded from https://onlinelibrary.wiley.com/doi/10.1002/aelm.202400908 by University Degli Studi Di Bari, Wiley Online Library on [04/02/2025]. See the Terms and Conditions (https://onlinelibrary.wiley.com/terms-and-conditions) on Wiley Online Library for rules of use; OA articles are governed by the applicable Creative Commons License

the Experimental Section, the sensing protocol involves recording 20 consecutive transfer curves for each tested solution. Only the final transfer curve for each solution is shown in Figure 2b, highlighting the stable current levels achieved during the measurement. The violet curve represents the baseline current (I_0) recorded after incubating the sensing gate for 10 min in a basic PBS solution. Following incubation, the sensing gate is rinsed with deionized (DI) water, placed in the measurement well, and subjected to cyclic testing step. Subsequently, it is immersed in 100 µL of PBS solution containing the oligonucleotide sequence matching that of the N sgRNA. The blue curve (I) reflects the current recorded after the binding of a single target strand, with measurements taken in water. Indeed, the sample comprises a PBS solution spiked with 10 zM (10^{-20} M) of oligonucleotide corresponding to N sgRNA. Additional transfer curves in Figure 2b were obtained by exposing the sensing gate to PBS solutions with target strands at concentrations of 100 zM, 1 aM, 10 aM, 100 aM, and 1 fM. For each solution, the relative current shift ($\Delta I/I_0 = (I-I_0)/I_0$) at $V_G = -0.4$ V, at the maximum transconductance, was calculated. Figure 2c presents a negative control experiment in which the biofunctionalized sensing gate, was exposed to PBS solutions containing the non-complementary target strand. This assay covered the same concentration range (from 10 zM to 1 fM), and the relative current shift (I relative to I_0) was similarly evaluated. The insets in Figure 2b,c display the gate leakage currents (I_G) within the V_G range of the sensing experiment. These curves, recorded at each stage of the experiment, illustrate the Faradaic I_G current contribution, which is over three orders of magnitude smaller than the I_D current flowing through the device. Additionally, there is no observable dependence of I_G on the tested cDNA standard solutions. Figure 2d presents the data from Figure 2b,c as dose-response curves of the SiMoT electronic signal $\Delta I/I_0$ for both the negative control (black circles) and the sensing experiment (blue squares) performed with the oligonucleotide corresponding to cDNA spiked PBS solutions. The SiMoT sensing response was modeled using an analytical approach (represented by the solid blue curve) based on Poisson distribution probabilities, as described in previous studies.[38,39] The model, encompassing a four-parameter logistic equation,[31] accounts for the limited number of binding events observed. The negative control experiments were employed to establish the average noise level of the assay, calculated as 0.06 ± 0.05. The limit of detection (LOD), defined as the noise level plus three times its standard deviation (0.20, indicated by the gray dashed line),[40] was determined to be 400 zM. Given that each sampled solution has a volume of 100 µL, the LOD corresponds to 24 ± 5 target strands. This demonstrates, with 99.73% confidence at the LOD, that the SiMoT assay is capable of detecting tens of target strands within a 100 µL sample volume. Additionally, the SiMoT current was recorded with the reference gate during each step of the assay to further validate the process.

As demonstrated in Figure 2d, the average relative current shift observed using the reference gate (red triangles) is 0.08 ± 0.02, which is significantly below the LOD threshold. In Figure 2e, the I_D current values at $V_G = -0.4$ V are presented as a function of time (bottom x-axis) and cycle number (top x-axis) for 20 consecutive transfer characteristic recordings. The first 320 s (corresponding to 20 cycles) represent the cycling protocol for the biofunctionalized gate after exposure to the reference fluid, highlighting the dynamic evolution of the baseline current over time. The following 320 s (cycles 21–40) show the signal response to a standard solution containing 1 aM of cDNA. From the curve in Figure 2e, it is possible to extract the most representative parameter of the system, selected to develop a machine-learning-based landmark analysis,[41,42] instead of directly feeding the classification algorithm with the entire current traces. Such an approach offers the main advantage of reducing computational complexity, enhancing the algorithm's efficiency, and potentially improves classification accuracy by focusing on the most informative features rather than processing redundant or noisy data from the full current traces.

Table 2. Summary of the SiMoT cohort comprising 90 samples.

	Positive patients	Negative patients	Samples spiked with N sgRNA	Samples spiked with non-complementary sgRNA	Total samples
Training set	14	4	19	23	60
Test set	16	14	–	–	30

Therefore, for each assayed solution the features $\Delta I/I_0$, ΔV_{th}, and $\Delta I/\Delta I_0$, described in detail in the Experimental Section, have been evaluated. The parameter $\Delta I/I_0$ quantifies the relative signal variation against the baseline, to minimize the effect of the device-to-device fluctuation, while ΔV_{th} represents the threshold voltage shift observed upon target sequence binding. Additionally, $\Delta I/\Delta I_0$ captures the normalized slope of current drift during signal cycling relative to the baseline. In other words, the $\Delta I/\Delta I_n$ feature represents the dynamic behavior of a given sensing gate. The current drift observed during stabilization is linked to the formation of the electric double layer at the electrode/electrolyte interface when the gate potential is applied, a process that is highly specific to each gate. The current dynamics, which reflect the adjustment of the biofunctionalized electrode to a lower ionic strength environment, are characteristic of the sensing gate. The cycling of the gate in the measuring well, whether it stabilizes within 20 cycles or not, reveals the rate of this stabilization process, being a key characteristic feature of each gate. Understanding and analyzing this dynamic behavior is highly informative for evaluating gate performance. In Figure 2e inset, ΔV_{th} is derived graphically from the $\sqrt{I_D}$ versus V_G plots (red curve for baseline, blue curve for signal), illustrating the shift upon exposure to the sampled solution. These metrics serve as features for subsequent machine learning landmark analysis (vide infra).

3. The Clinical Assay on COVID-19 Patients

The SiMoT sensing protocol was utilized to analyze the presence of N sgRNA in RNA extracted from residual nasopharyngeal swab samples of 30 SARS-CoV-2-positive individuals and 18 SARS-CoV-2-negative individuals, as summarized in **Table 2**. Each sample was initially characterized by droplet digital PCR (ddPCR) assays, to precisely detect the presence of SARS-CoV-2 gRNA and quantify the content of N sgRNA. Typical data measured for SARS-CoV-2-positive and negative samples are presented in **Figure 3**a,b, respectively. Figure 3a illustrates the time-resolved drain current (I_D) levels measured at $V_G = -0.4$ V, along with the corresponding transfer characteristic recorded during

© 2025 The Author(s). Advanced Electronic Materials published by Wiley-VCH GmbH

2199160x, 0, Downloaded from https://onlinelibrary.wiley.com/doi/10.1002/aelm.202400908 by University Degli Studi Di Bari, Wiley Online Library on [04/02/2025]. See the Terms and Conditions (https://onlinelibrary.wiley.com/terms-and-conditions) on Wiley Online Library for rules of use; OA articles are governed by the applicable Creative Commons License

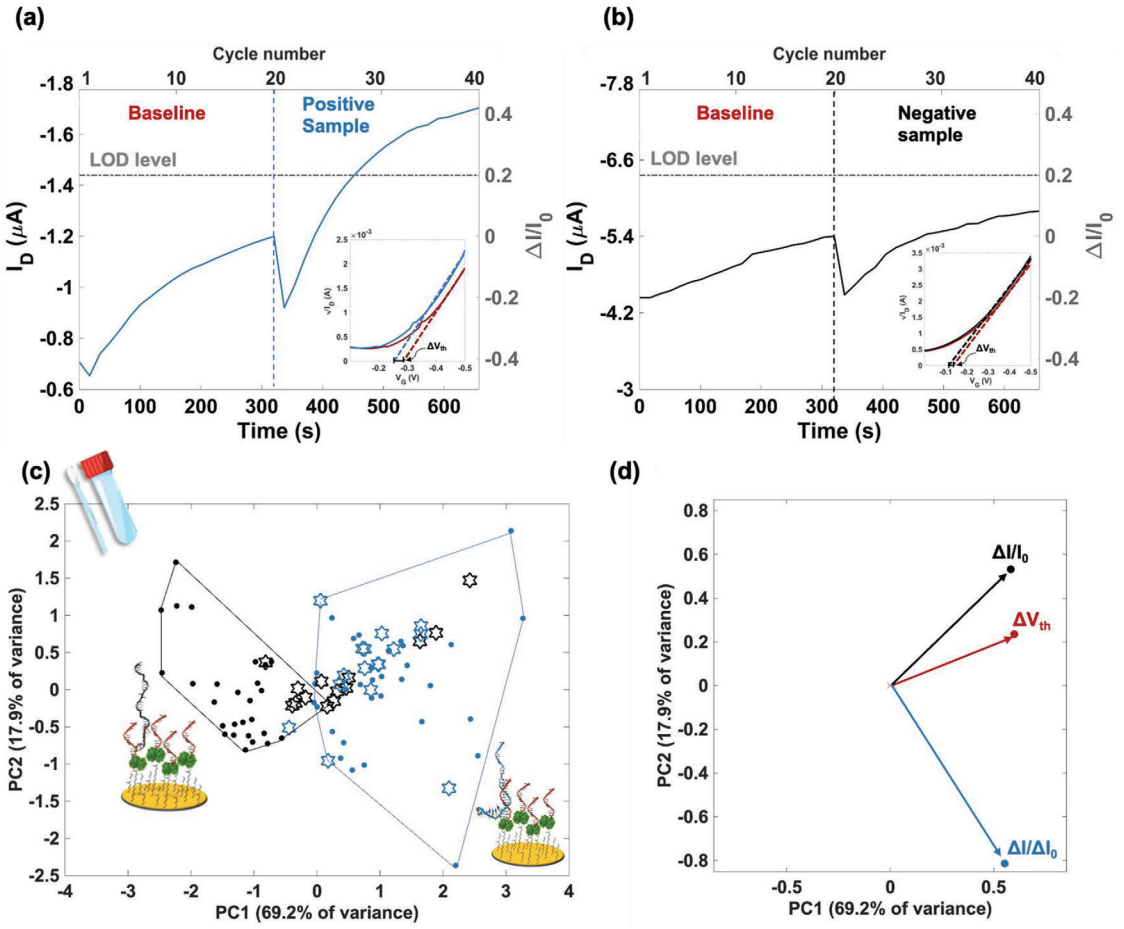

Figure 3. a) Time-resolved I_D measurements at $V_G = -0.4$ V, recorded before and after exposure to a patient's RNA tested as positive for SARS-CoV2 gRNA and N sgRNA. The inset shows the $\sqrt{I_D}$ as a function of the gate bias, showing the typical threshold voltage shift registered between the baseline (red curve) and the signal (blue curve). b) Time-resolved I_D measurements at $V_G = -0.4$ V, recorded before and after exposure to a patient's RNA tested as negative for SARS-CoV2 gRNA and N sgRNA. The inset shows the $\sqrt{I_D}$ versus V_G, showing the typical threshold voltage shift registered between the baseline (red curve) and the signal (black curve). c) Score–Plot illustrating the scores of the samples assessed using the SiMoT assay. The blue samples are the N sgRNA positives, while those in black indicate the N sgRNA negative samples. The points represent the samples of the training set, used to compute the PCs, while the hollow stars are the samples belonging to the test set, projected on the PCA model. d) The loading plot shows the contributions of each initial variable extracted for the SiMoT assay on principal components PC1 and PC2. The loading of the variables $\Delta I/I_0$, ΔV_{th}, and $\Delta I/\Delta I_0$ are shown as black, red, and blue arrows, respectively.

the final cycle, both before and after incubation in a COVID-19 positive patient sample. The ddPCR also detected as few as 2.00 ± 0.14 copies per reaction of N sgRNA in a 5 µL sample volume, thus corresponding to a concentration of 600 zM. The very same patient sample assayed with the SiMoT technology, returned a distinct signal change, expressed as $\Delta I/I_0$, of 0.41, being well above the LOD, upon sensing the 600 zM of N sgRNA. Furthermore, as shown in the inset of Figure 3a, a significant threshold voltage shift of 24 ± 3 mV is observed. This suggests that the sensing gate experiences a sizable work function change upon the binding of 36 ± 6 target strands in 100 µL sample volume. In contrast, the COVID-19 negative sample, confirmed by ddPCR for the N sgRNA, exhibited a signal change ($\Delta I/I_0$) of 0.08, which was below the LOD. Additionally, it showed a negligible ΔV_{th} of 5 ± 3 mV, as illustrated in Figure 3b. The complete dataset, characterized for N sgRNA using the SiMoT assay, was initially examined through exploratory multivariate analysis employing Principal Component Analysis (PCA), as showed in Figure 3c,d.

PCA generates a set of orthogonal principal components (PCs), with each component expressed as a linear combination of the variables $\Delta I/I_0$, ΔV_{th}, and $\Delta I/\Delta I_0$, weighted by the eigenvalues of the loading matrix. The scores reflect the cumulative contribution of each variable to a given PC. Additional details regarding the PCA methodology are documented elsewhere.[21,31,43] In this analysis PC1 and PC2, the first two principal components, effectively capture the dataset's variability, accounting for 87.1% of the total variance across the three features evaluated for each patient fluid sample. A total of 60 samples were utilized as the training set, while the remaining 30 samples were analyzed in a double-blind manner as the external test set, as summarized in Table 2. The training set, used to develop the PCA model, consisted of 33 positive and 27 negative samples.

 © 2025 The Author(s). Advanced Electronic Materials published by Wiley-VCH GmbH

2199160x, 0, Downloaded from https://onlinelibrary.wiley.com/doi/10.1002/aelm.202400908 by University Degli Studi Di Bari, Wiley Online Library on [04/02/2025]. See the Terms and Conditions (https://onlinelibrary.wiley.com/terms-and-conditions) on Wiley Online Library for rules of use; OA articles are governed by the applicable Creative Commons License

Table 3. SiMoT classifier's output on the external test set benchmarked against the results of COVID 19 molecular diagnosis and N sgRNA copies/ddPCR reaction.

Sample ID	gRNA molecular diagnosis	N sgRNA copies/ddPCR reaction	SiMoT classification	$\Delta I/I_0$	ΔV_{th} [mV]	$\Delta I/\Delta I_0$
24	N	0.00 ± 0.00	N	0.35	4	1.73
F	N	0.00 ± 0.00	N	0.24	3	0.35
5	N	0.00 ± 0.00	N	0.35	7	1.29
8	N	0.00 ± 0.00	N	0.36	6	1.72
12	N	0.00 ± 0.00	N	0.32	1	1.36
20	N	0.00 ± 0.00	N	0.37	8	1.61
1	N	0.00 ± 0.00	N	0.24	4	1.24
14	N	0.00 ± 0.00	N	0.26	3	1.26
2	N	0.00 ± 0.00	N	0.31	1	1.14
9	N	0.00 ± 0.00	P	0.58	30	1.84
4	N	0.00 ± 0.00	P	0.40	14	1.53
7	N	0.00 ± 0.00	P	0.69	23	2.04
15	N	0.00 ± 0.00	P	0.77	41	1.61
18	N	0.00 ± 0.00	P	0.39	11	1.66
30	P	32.00 ± 11.70	N	0.18	6	1.45
13	P	2219.00 ± 76.60	P	0.60	30	1.77
23	P	17.00 ± 0.28	P	0.48	9	2.05
3	P	2019.00 ± 79.80	P	0.37	37	1.48
6	P	58.00 ± 5.29	P	0.63	27	1.70
21	P	2293.00 ± 141.20	P	0.35	40	1.43
25	P	1835.00 ± 56.00	P	0.42	26	1.21
22	P	1380.00 ± 42.30	P	0.51	25	1.29
26	P	44.70 ± 9.45	P	0.37	27	0.03
10	P	53.00 ± 11.00	P	0.28	27	1.33
17	P	1157.00 ± 182.90	P	0.48	31	1.57
29	P	93.00 ± 4.62	P	0.23	7	2.37
19	P	2.00 ± 0.14	P	0.41	24	1.50
28	P	23.00 ± 4.38	P	0.28	31	1.22
D	P	3.00 ± 0.28	P	0.45	24	4.15
E	P	76.00 ± 8.72	P	0.37	5	1.13

The training set positive class included 14 samples from COVID-19 positive patients, and 19 samples spiked with N sgRNA at concentrations above the LOD, thus ranging from 1 aM to 1 fM. Conversely, the training set negative class comprised 4 samples from COVID-19 negative patients and 23 samples spiked with a non-complementary sgRNA strand. This design ensured a balanced distribution of negative and positive samples in the training set. Figure 3c illustrates the scores for PC1 and PC2 calculated using the training set samples. Specifically, the blue points represent scores from positive samples, while the black points correspond to negative samples within the training set. The score plot reveals distinct clustering, with positive samples aligning at higher PC1 values and negative samples displaying negative PC1 scores. Moreover, Figure 3d presents the loadings for PC1 and PC2, highlighting the contribution of the original variables to the principal components. The loading plot demonstrates that all three features, which increase in value in the presence of the target strands, contribute positively to the loadings on PC1. The hollow stars in Figure 3c represent the patient samples from the external test set. These samples were projected onto the PCA model, showing a general alignment with the clusters observed in the training set. However, a region of overlap is evident in the score plot.

To achieve a clear binary classification between N sgRNA-positive and negative samples, a machine learning approach was applied.[44,45] Specifically, a K-Nearest Neighbor (*K-NN*) classifier was trained on the training set (60 samples), and its performance was estimated on an external test set (30 samples). To avoid overfitting, the test set was excluded from the training phase. As standard practice, the *K-NN* decision boundary was assessed through 10 iterations of cross-validation.[21,46] All samples in the training-set were correctly classified by the *K-NN* classifier, in line with the results from ddPCR. To further evaluate the model's predictive performance, the trained *K-NN* classifier was applied to classify the samples in the external test set using a double-blind approach. The results, presented in **Table 3**, compare the classifier's results with the ddPCR findings for gRNA and N sgRNA. The SiMoT classifier misclassified six samples, as shown in red in Table 3. Specifically, one positive sample was incorrectly classified as negative, resulting in one false negative across the 90

© 2025 The Author(s). Advanced Electronic Materials published by Wiley-VCH GmbH

2199160x, 0, Downloaded from https://onlinelibrary.wiley.com/doi/10.1002/aelm.202400908 by University Degli Studi Di Bari, Wiley Online Library on [04/02/2025]. See the Terms and Conditions (https://onlinelibrary.wiley.com/terms-and-conditions) on Wiley Online Library for rules of use; OA articles are governed by the applicable Creative Commons License

samples. Additionally, five negative samples were misclassified as positive, resulting in five false positives. As a result, the diagnostic sensitivity (the percentage of true positives correctly identified) and diagnostic specificity (the percentage of true negatives correctly identified) for the entire cohort were 98.0% and 87.8%, respectively. Notably, these results were obtained using portable equipment suitable for point-of-care settings, delivering results in just 30 min at an estimated cost of less than 10 €. In contrast, standard diagnostic methods, based on PCR, take up to 6 h and can cost several hundred euros.

4. Conclusion

The SiMoT portable bioelectronic platform is proposed as a novel tool for detecting sgRNAs. The SiMoT prototype, developed at Technology Readiness Level 5 (TRL5), reliably detects sgRNA encoding the nucleocapsid (N) protein with a LOD as low as 400 zM, corresponding to 24 ± 5 strands in a 100 µL sample volume. The N sgRNA strands are directly detected in RNA extracted from nasopharyngeal swab samples from SARS-CoV-2 patients.

A machine-learning-based classifier trained on data from 60 samples was tested with an external, double-blind set of 30 patient samples. Remarkably, the SiMoT assay achieved 98% diagnostic sensitivity and 87.8% diagnostic specificity across all 90 samples analyzed. Furthermore, SiMoT is faster and more cost-effective than the current state-of-art diagnostic techniques, making it the sole assay fully compatible with point-of-care (POC) settings.

Therefore, the SiMoT technology represents a groundbreaking approach to detecting active viral replication, addressing the limitations of existing methods. Its high sensitivity, good specificity, rapid turnaround time, and affordability establish it as a reliable diagnostic tool for SARS-CoV-2 and other coronaviruses. Additionally, the simplicity and scalability of the platform enable widespread adoption in both clinical and resource-limited settings. SiMoT has the potential to revolutionize global diagnostic capabilities, particularly in managing ongoing and future pandemics.

5. Experimental Section

Materials: The following chemicals were obtained from Sigma–Aldrich: Poly(3-hexylthiophene-2,5-diyl) (P3HT, molecular weight of 17.5 kDa), 3-mercaptopropionic acid (3MPA), 11-mercaptoundecanoic acid (11MUA), N-hydroxysulfosuccinimide sodium salt (NHSS), 1-ethyl-3-(3-dimethylaminopropyl)carbodiimide (EDC), and Ethanolamine hydrochloride (EA). Phosphate-buffered saline (PBS) tablets were dissolved in HPLC water and filtered using a 0.22 µm Corning polyethersulfone membrane. Neutravidin and Bovine Serum Albumin (BSA) were also purchased from Sigma–Aldrich. The biotinylated single-strand oligonucleotide sequence (b-DNA) 5′-CATTTTAGTTTGTTCGTTTAGA-3′, the target oligonucleotide (5′-GGTAACAAACCAACCAACTTTCGATCTCTTGTAGATCTGTTCTCTAAACGAACAAACTAAAATGTCTGATAATGGACCCCAAAATCAGCGAAATGCACCC-3′) and the non-complementary oligonucleotide (5′-AGACCTTAAATTCCCTCGAGGACAAGGCGTTCCAATTAACACCAATAGCAGTCCAGATGACCAAATTGGCTACTACCGAAGAGCTACCAGACGAATTCGT-3′) were synthetized by Invitrogen.

Biofunctionalization Protocol: A SAM is deposited on the gold detecting interface by depositing a solution with 10 mM of 3-MPA and 11-MUA (in a 10:1 molar ratio) dissolved in ethanol. The gold surface is then activated using a 200 m M solution of EDC with a 50 m M sulfo-N-hydroxysuccinimide (sulfo-NHS) aqueous solution at 25 °C for 20 min. The activated surface is then exposed to a neutravidin solution (100 µg mL^{-1}) for 1.5 h. Then, the surface is exposed to the biotinylated single-strand oligonucleotide sequence (b-DNA) 5′-CATTTTAGTTTGTTCGTTTAGA (0.5 µM) for 1 h.

Biomarker's Standard Solutions in PBS: PBS standard solutions of the analyte oligonucleotide sequences were prepared using a standard serial dilution protocol. The nominal concentrations used for SPR characterization range from 10^{-8} to 8×10^{-7} M, while for SiMoT validation, they range from 1×10^{-20} to 10^{-15} M. The PBS solution, which mimics a physiological environment, maintains an ionic strength and a pH of 162 mM and 7.4, respectively. The target single-strand oligonucleotide and the non-complementary oligonucleotide, used for the negative control experiment are both 100 bases long.

Collection of Patients' Samples: Remnants from nasopharyngeal swabs (in UTM matrix) from of unidentified subjects were collected at the Istituto Zooprofilattico Sperimentale della Puglia e Basilicata, Putignano, Italy. 560 µL of UTM matrix were used to purify viral RNA using the QIAamp Viral RNA Mini Kit (Qiagen, Hilden, German) according to the manufacturer's instructions. RNA samples were analyzed by an in-house reverse transcription-qPCR assay using the primers/probe for N gene, as from the World Health Organization, previously described previously.[47] to confirm the presence of the viral RNA. 30 RNA samples were identified as positive and 18 were identified as negative for SARS-CoV-2. Ethical approval was not required for this study, as nasopharyngeal swab remnants were from subjects that remained unidentified, and data generated concerned exclusively viral sequences. RNA samples were stored at −80 °C until use. The quantification of N sgRNA was performed by Reverse Transcription (RT) followed by droplet digital PCR (ddPCR).[3] Briefly, 10 ng of viral RNA was reverse transcribed into cDNA using the iScript Reverse Transcription Supermix for RT-qPCR (Bio-Rad, Hercules, CA, USA) according to the manufacturer's instructions. The ddPCR reaction was set up with a final volume of 22 µL, combining 1 µL of the cDNA with 11 µL of 2X Evagreen Supermix (Bio-Rad), primers LS_For1 and N_Rev at 250 nM final concentration and water. All samples were assayed in analyzed in triplicate and a negative control (no template control) was included in each experiment. The emulsion was generated using the QX200 Droplet Generator (Bio-Rad) according to the manufacturer's instructions. Then the droplet partitioned samples were amplified, according to already reported amplification profile.[3] Absolute quantification was performed using the QuantaSoft version 7.4.1 software (Bio-Rad) and the negative/positive thresholds were set manually. The absolute quantification of each target was expressed in copies/µL of ddPCR reaction.

The N sgRNA analysis was accomplished ensuring all procedures were performed under RNAse-free conditions. The water used for RNA handling was RNase-free to prevent RNA degradation by RNases. To this aim, HPLC water was treated with diethyl pyrocarbonate (DEPC), chemical agent that inactivates RNases. The treatment involves adding DEPC at a concentration of 0.1% v/v to the water, followed by incubation stirring overnight at 25 °C. Subsequently, the water is sterilized by autoclaving for 20 min, following the inactivation of any remaining traces of DEPC. Before the sensing measure, the samples were diluted 1:4 (v/v) in RNAse-free phosphate-buffered saline (PBS). Next, an aliquot of each diluted sample was incubated in a water bath at 60 °C for 10 min, followed by immediate cooling on ice for 1 min before incubation with the biofunctionalized gate.

Surface Plasmon Resonance Characterization: SPR data are collected using a BioNavis-200 Multi-Parameter Surface Plasmon Resonance (MP-SPR) Navi instrument in the Kretschmann configuration. Piranha solution was used for the cleaning procedures of SPR sensor slides. Substrates were immersed for 10 min in NH_3/H_2O_2 aqueous solution (1:5 v/v) for 10 min at a temperature of 80–90 °C. Then, substrates were rinsed with water, dried with nitrogen, and treated in a UV–ozone cleaner for 10 min. The SPR slide, docked in a 100 µL flow-through cell, consists of a gold coated optical glass matching the high refractive index of the prism on which the laser beam strikes. The solutions are injected manually in batches of 100 µL. The SPR apparatus is equipped with two laser beams that

© 2025 The Author(s). Advanced Electronic Materials published by Wiley-VCH GmbH

2199160x, 0, Downloaded from https://onlinelibrary.wiley.com/doi/10.1002/aelm.202400908 by University Degli Studi Di Bari, Wiley Online Library on [04/02/2025]. See the Terms and Conditions (https://onlinelibrary.wiley.com/terms-and-conditions) on Wiley Online Library for rules of use; OA articles are governed by the applicable Creative Commons License

simultaneously inspect two different points (3 mm apart) of the detecting interface, to assess the uniformity of the film over the 0.4 cm^2 area inspected. The two traces measured concur to the number of replicates acquired for a given experiment. The laser incident angle θ is varied in the 50.290°–77.930° range with an instrumental error of $1 \cdot 10^{-3}$ (°) corresponding to one unit shift in the SPR reflectance intensity, while a θ shift of 86.3 (°) corresponds to one refractive index unit. All the experiments are performed at 21.0 ± 0.1 °C. The measured sensograms are the plasmon resonant angle θ_{SPR} versus time. The SPR characterization is conducted monitoring the detecting surface in situ and real-time.

SiMoT Fabrication and Electronic Characterization: The SiMoT platform was fabricated, as described in detail elsewhere,[30,38,48] beginning with a Si/SiO_2 substrate patterned with photo-lithographically defined drain (D) and source (S) interdigitated electrodes (e-beam evaporation, with 5 nm of Ti and 50 nm of Au).

Two circular electrodes (≈0.2 cm^2) were fabricated on a PEN foil by e-beam evaporation of Au, serving as the reference and sensing gates. The b-DNA single strand was used to biofunctionalize the sensing gate, while the reference gate was left unmodified. This reference gate allows continuous monitoring of the channel current, ensuring the stability of the device throughout the assay. To this aim, the reference gate always remains in the measurement well.

The sensing measurement protocol begins by stabilizing the FET channel current, using the reference gate. This process continues until a stable current is observed over three consecutive cycles. Subsequently, the sensing gate is exposed for 10 min to 100 µL of reference fluid (PBS solution). Afterward, it is washed with HPLC-grade water, positioned into the measurement well, and the first 20 transfer characteristics are recorded. Once 20 cycles are completed and a stable baseline current (I0) is achieved, the sensing gate is extracted from the measurement well and repositioned in the incubation well with 100 µL of PBS solutions with the target DNA complementary strand or the endogenous N sgRNA in the patient's RNA. Negative control experiments are conducted using PBS with a non-complementary DNA strand as the sample. After 10 min, the sensing gate is washed again, returned to the measurement well, and another 20 transfer characteristics are recorded, referred to as the signal current (I).

SiMoT Classification Model: The SiMoT assay provides a binary, yes/no response utilizing a machine learning approach, specifically the *K-Nearest Neighbors* (K-NN) algorithm.[44,49] The binary classifier was trained on a dataset comprising 33 positive samples, including 19 PBS standard solutions spiked with the target oligonucleotide sequence and 14 RNAs from COVID 19 positive samples. It also included 27 negative samples, consisting of 23 PBS standard solutions spiked with a non-complementary oligonucleotide sequence and 4 RNAs from COVID 19 negative samples. Those 60 analyses were employed to train the model. Moreover, a test set consisting of 30 swab samples (in double-blind manner), was utilized to evaluate the performances of the classification model. The summary of the measurements performed on the test set is given in Table 3, along with the output of the classification model and the diagnosis achieved through ddPCR is given as well. For RNA samples analyzed trough the SiMoT assay, the following features were calculated: *i)* $\boldsymbol{\Delta I/I_0} = (I_{15-20} - I_{0\_15-20})/I_{0\_15-20}$ (average over three replicates), where $I_{15-20} = \frac{1}{5}\sum_{i=15}^{20} I \cdot (V_G = -0.4\ V;\ V_D = -0.4\ V)$ is the sensing current averaged over cycles 15–20 after the sensing gate incubation in a patient sample, while the $I_{0,\_15-20} = \frac{1}{5}\sum_{i=15}^{20} I_0 (V_G = -0.4\ V;\ V_D = -0.4\ V)$ is the baseline current averaged (cycles 15–20) after exposure to the PBS reference fluid. *ii)* $\boldsymbol{\Delta V_{th}} = V_{th} - V_{th0}$ is the threshold voltage shift measured upon exposure to the patient sample. The latter was extracted from the equation describing the I_D current flowing in the transistor channel in the saturation regime,[50] given by the following equation $I_D = \frac{W\mu_{FET}C_i}{2L}(V_G - V_{th})^2$, where L is the channel length and W is the channel width, while C_i is the capacitance per unit area of the gating system, V_{th} is the threshold voltage, and μ_{FET} is the field-effect mobility. From the equation previously mentioned, $\sqrt{I_D}$ is linearly related to $(V_G - V_{th})$, with V_{th} corresponding to the intercept on the V_G axis, while the product $(Ci \bullet \mu_{FET})$ is proportional to the slope of the linear segment of the curve. A V_{th} shift after exposure to the target analyte evidences an adjustment in the electrochemical potential or work function of the gate, reflecting the biorecognition events.[35] The threshold voltages before and after exposure to the patient samples, used to compute the ΔV_{th} feature, are the average values recorded over the last 5 cycling steps. *iii)* $\boldsymbol{\Delta I/\Delta I_0} = \frac{I_{20} - I_1}{I_{0,20} - I_{0,1}}$, where I_1, I_{20}, $I_{0,1}$ $I_{0,20}$ are the baseline (I) and the sensing (I_0) current values (at $V_G = -0.4$ V and $V_D = -0.4$ V) registered during the cycles 1 and 20. It is related to the normalized dynamic drift of a specific sensing gate. A schematic depiction of the features is shown in Figure 2e. The K-NN classifier was trained using those three features extracted from each assay in the training set. This algorithm operates on a *guilt by association* concept, where the classification result is achieved by assessing the similarity between a new query and patterns in the training set, based on calculated distances. As a non-linear discriminant classification method, it categorizes a query object by evaluating its distances to all objects in the training set. The query is then assigned to the category of the k-nearest-neighbors, with the value of k indicating the number of neighboring objects considered in determining its classification. The *K-Nearest Neighbors* algorithm for the SiMoT dataset was performed with a value of k set to 3 to prevent ties in classification, using Euclidean distance as the metric. To fine-tune the K-NN model, a 10-fold cross-validation was conducted. The K-NN classifier was implemented using the freely available software *Chemometric Agile Tool* (CAT).[51]

The specificity and sensitivity of the model were calculated as:

$$Specificity = \frac{TN}{TN + FP} \cdot 100\% = 100\% \quad (1)$$

$$Sensitivity = \frac{TP}{TP + FN} \cdot 100\% = 100\% \quad (2)$$

where TN and TP represent the numbers of true negatives and true positives, while FP and FN represent the numbers of false positives and false negatives, respectively.

Acknowledgements

The authors thank Dr. Annunziata De Luisi and Dr. Petronilla Frugis for their laboratory support. The Centro di Innovazione Regionale Digital Assay, Regione PUGLIA Delibera Regionale n 702 del 08/11/2022 CUP B93C22000840001; NoOne-A binary sensor with single-molecule digit to discriminate biofluids enclosing zero or at least one biomarker, ERC Stg2021, GA:101040383; PRIN project prot.2017RHX2E4 "At the forefront of Analytical ChemisTry: disrUptive detection technoLogies to improve; Italian network of excellence for advanced diagnosis (INNOVA), Ministero della Salute-code PNC-E3-2022-23683266 PNC-HLS-DA, CUP: C43C22001630001; Complementary National Plan PNC-I.1 "Research initiatives for innovative technologies and pathways in the health and welfare sector" D.D. 931 of 06/06/2022, DARE—DigitAl lifelong pRevEntion initiative, code PNC0000002, CUP: B53C22006420001; Tecnologie portatili e protocolli innovativi per la diagnosi ultrasensibile di Xylella fastidiosa direttamente in piante e vettori (1LIVEXYLELLA) Ministero dell'agricoltura, della sovranità alimentare e delle foreste—MIPAAF D.M. n.419161 del 13/09/2022; Research actions for reducing the impact on agricultural and natural ecosystems of the harmful plant pathogen Xylella fastidiosa (REACH-XY)—CUP B93C22001920001; the National Center for Gene Therapy and Drugs Based on RNA Technology (Project no. CN_00000041) and ELIXIR-IT through the empowering project ELIXIRNextGenIT (Grant Code IR0000010) are acknowledged for partial financial support.

Conflict of Interest

The authors declare no conflict of interest.

Data Availability Statement

The data that support the findings of this study are available from the corresponding author upon reasonable request.

© 2025 The Author(s). Advanced Electronic Materials published by Wiley-VCH GmbH

2199160x, 0, Downloaded from https://onlinelibrary.wiley.com/doi/10.1002/aelm.202400908 by University Degli Studi Di Bari, Wiley Online Library on [04/02/2025]. See the Terms and Conditions (https://onlinelibrary.wiley.com/terms-and-conditions) on Wiley Online Library for rules of use; OA articles are governed by the applicable Creative Commons License

Keywords

bioelectronics, biomarkers, early-detections, SiMoT, subgenomic RNA

Received: December 2, 2024
Revised: January 8, 2025
Published online:

[1] G. Dagotto, N. B. Mercado, D. R. Martinez, Y. J. Hou, J. P. Nkolola, R. H. Carnahan, J. E. Crowe, R. S. Baric, D. H. Barouch, *J. Virol.* **2021**, *95*, e02370.
[2] A. R. Fehr, S. Perlman, in *Coronaviruses: Methods and Protocols*, (Eds: H. J. Maier, E. Bickerton, P. Britton), Springer, New York, NY, **2015**, pp. 1–23.
[3] A. Oranger, C. Manzari, M. Chiara, E. Notario, B. Fosso, A. Parisi, A. Bianco, M. Iacobellis, M. d'Avenia, A. M. D'Erchia, G. Pesole, *Commun. Biol.* **2021**, *4*, 1215.
[4] P. Cohen, E. J. DeGrace, O. Danziger, R. S. Patel, E. A. Barrall, T. Bobrowski, T. Kehrer, A. Cupic, L. Miorin, A. García-Sastre, B. R. Rosenberg, *Microbiol. Spectr.* **2023**, *11*, e00776.
[5] B. A. Oliveira, L. C. de Oliveira, E. C. Sabino, T. S. Okay, *Rev. Inst. Med. Trop.* **2020**, *62*, e44.
[6] K. Okamaoto, K. Shirato, N. Nao, S. Saito, T. Kageyama, H. Hasegawa, T. Suzuki, S. Matsuyama, M. Takeda, *Jpn. J. Infect. Dis.* **2020**, *73*, 366.
[7] A. Afzal, *J. Adv. Res.* **2020**, *26*, 149.
[8] S. G. Sawicki, D. L. Sawicki, S. G. Siddell, *J. Virol.* **2007**, *81*, 20.
[9] R. Lambkin-Williams, J. P. DeVincenzo, *Influenza Resp. Viruses* **2020**, *14*, 747.
[10] R. Lambkin-Williams, N. Noulin, A. Mann, A. Catchpole, A. S. Gilbert, *Respir. Res.* **2018**, *19*, 123.
[11] https://doi.org/10.1128/jvi.00100-23.
[12] S. Long, *Viruses* **2021**, *13*, 1923.
[13] https://www.thelancet.com/journals/laninf/article/PIIS1473-3099(20)30314-5/fulltext.
[14] R. A. Perera, E. Tso, O. T. Tsang, D. N. Tsang, K. Fung, Y. W. Leung, A. W. Chin, D. K. Chu, S. M. Cheng, L. L. Poon, V. W. Chuang, M. Peiris, *Emerg. Infect. Dis.* **2020**, *26*, 2701.
[15] X. Ge, H. Zhou, F. Shen, G. Yang, Y. Zhang, X. Zhang, H. Li, *Clin. Chem. Lab. Med.* **2024**, *62*, 1019.
[16] R. Wölfel, V. M. Corman, W. Guggemos, M. Seilmaier, S. Zange, M. A. Müller, D. Niemeyer, T. C. Jones, P. Vollmar, C. Rothe, M. Hoelscher, T. Bleicker, S. Brünink, J. Schneider, R. Ehmann, K. Zwirglmaier, C. Drosten, C. Wendtner, *Nature* **2020**, *581*, 465.
[17] Y. Li, L. Yao, J. Li, L. Chen, Y. Song, Z. Cai, C. Yang, *J. Med. Virol.* **2020**, *92*, 903.
[18] J. Y. Kim, J.-Y. Bae, S. Bae, H. H. Cha, J.-S. Kwon, M. H. Suh, H. J. Lee, J. Jung, M. J. Kim, C. Cui, H. Park, J. Lee, M.-S. Park, S.-H. Kim, *Clin. Microbiol. Infect.* **2022**, *28*, 101.
[19] E. Macchia, F. Torricelli, M. Caputo, L. Sarcina, C. Scandurra, P. Bollella, M. Catacchio, M. Piscitelli, C. Di Franco, G. Scamarcio, L. Torsi, *Adv. Mater.* **2024**, *36*, 2309705.
[20] E. Macchia, Z. M. Kovács-Vajna, D. Loconsole, L. Sarcina, M. Redolfi, M. Chironna, F. Torricelli, L. Torsi, *Sci. Adv.* **2022**, *8*, eabo0881.
[21] E. Genco, F. Modena, L. Sarcina, K. Björkström, C. Brunetti, M. Caironi, M. Caputo, V. M. Demartis, C. Di Franco, G. Frusconi, L. Haeberle, P. Larizza, M. T. Mancini, R. Österbacka, W. Reeves, G. Scamarcio, C. Scandurra, M. Wheeler, E. Cantatore, I. Esposito, E. Macchia, F. Torricelli, F. A. Viola, L. Torsi, *Adv. Mater.* **2023**, *35*, 2304102.
[22] K. T. Desai, K. Alfaro, L. Mendoza, M. Faron, B. Mesich, M. Maza, R. Dominguez, A. Valenzuela, C. D. Acosta, M. Martínez, J. C. Felix, R. Masch, J. S. Smith, S. Gabrilovich, T. Wu, M. Plump, A. P. Novetsky, M. H. Einstein, N. C. Douglas, M. Cremer, N. Wentzensen, *Microbiol Spectr* **2021**, *9*, e00846.
[23] J. C. Zhou, B. Feller, B. Hinsberg, G. Sethi, P. Feldstein, J. Hihath, E. Seker, M. Marco, A. Knoesen, R. Miller, *Colloids Surf. A* **2015**, *481*, 72.
[24] E. Macchia, F. Torricelli, P. Bollella, L. Sarcina, A. Tricase, C. Di Franco, R. Österbacka, Z. M. Kovács-Vajna, G. Scamarcio, L. Torsi, *Chem. Rev.* **2022**, *122*, 4636.
[25] L. Sarcina, E. Macchia, G. Loconsole, G. D'Attoma, P. Saldarelli, V. Elicio, G. Palazzo, L. Torsi, *Ad. NanoBiomed. Res.* **2021**, *1*, 2100043.
[26] L. Sarcina, C. Scandurra, C. Di Franco, M. Caputo, M. Catacchio, P. Bollella, G. Scamarcio, E. Macchia, L. Torsi, *J. Mater. Chem. C* **2023**, *11*, 9093.
[27] B. Holzer, K. Manoli, N. Ditaranto, E. Macchia, A. Tiwari, C. Di Franco, G. Scamarcio, G. Palazzo, L. Torsi, *Adv. Biosys.* **2017**, *1*, 1700055.
[28] J. A. De Feijter, J. Benjamins, F. A. Veer, *Biopolymers* **1978**, *17*, 1759.
[29] https://doi.org/10.1021/ja9719586.
[30] E. Macchia, K. Manoli, B. Holzer, C. Di Franco, M. Ghittorelli, F. Torricelli, D. Alberga, G. F. Mangiatordi, G. Palazzo, G. Scamarcio, L. Torsi, *Nat. Commun.* **2018**, *9*, 3223.
[31] C. Scandurra, K. Björkström, M. Caputo, L. Sarcina, E. Genco, F. Modena, F. A. Viola, C. Brunetti, Z. M. Kovács-Vajna, C. D. Franco, L. Haeberle, P. Larizza, M. T. Mancini, R. Österbacka, W. Reeves, G. Scamarcio, M. Wheeler, M. Caironi, E. Cantatore, F. Torricelli, I. Esposito, E. Macchia, L. Torsi, *Adv. Sci.* **2024**, *11*, 2308141.
[32] J. N. Weiss, *FASEB J.* **1997**, *11*, 835.
[33] L. Vanjur, T. Carzaniga, L. Casiraghi, M. Chiari, G. Zanchetta, M. Buscaglia, *Biophys. J.* **2020**, *119*, 989.
[34] https://doi.org/10.1021/am4011429.
[35] C. Di Franco, E. Macchia, L. Sarcina, N. Ditaranto, A. Khaliq, L. Torsi, G. Scamarcio, *Adv. Mater. Inter.* **2023**, *10*, 2201829.
[36] C. Di Franco, M. Piscitelli, E. Macchia, C. Scandurra, M. Catacchio, L. Torsi, G. Scamarcio, *J. Mater. Chem. C* **2024**, *12*, 73.
[37] C. Di Franco, E. Macchia, M. Catacchio, M. Caputo, C. Scandurra, L. Sarcina, P. Bollella, A. Tricase, M. Innocenti, R. Funari, M. Piscitelli, G. Scamarcio, L. Torsi, *Adv. Sci.* **2025**, *12*, 2412347.
[38] E. Macchia, A. Tiwari, K. Manoli, B. Holzer, N. Ditaranto, R. A. Picca, N. Cioffi, C. Di Franco, G. Scamarcio, G. Palazzo, L. Torsi, *Chem. Mater.* **2019**, *31*, 6476.
[39] L. Sarcina, E. Macchia, G. Loconsole, G. D'Attoma, P. Bollella, M. Catacchio, F. Leonetti, C. Di Franco, V. Elicio, G. Scamarcio, G. Palazzo, D. Boscia, P. Saldarelli, L. Torsi, *Adv. Sci.* **2022**, *9*, 2203900.
[40] M. Thompson, S. L. R. Ellison, R. Wood, *Pure Appl. Chem.* **2002**, *74*, 835.
[41] R. Vitale, O. E. De Noord, A. Ferrer, *Chemom. Intell. Lab. Syst.* **2015**, *149*, 40.
[42] K. T. Tanner, L. D. Sharples, R. M. Daniel, R. H. Keogh, *J. Royal Stat. Soc. Series A* **2021**, *184*, 3.
[43] E. Macchia, K. Björkström, A. Tewari, V. Eskonen, A. Luukkonen, A. M. Ghafari, L. Sarcina, M. Caputo, N. Tong-Ochoa, K. Kopra, F. Pettersson, Z. Gounani, L. Torsi, H. Härmä, R. Österbacka, *Cell Rep. Phys. Sci.* **2024**, *5*, 101874.
[44] P. Oliveri, G. Downey, *TrAC* **2012**, *35*, 74.
[45] https://www.sciencedirect.com.$^{-1}$science/article/abs/pii/B9780128-132661000024.

© 2025 The Author(s). Advanced Electronic Materials published by Wiley-VCH GmbH

2199160x, 0, Downloaded from https://onlinelibrary.wiley.com/doi/10.1002/aelm.202400908 by University Degli Studi Di Bari, Wiley Online Library on [04/02/2025]. See the Terms and Conditions (https://onlinelibrary.wiley.com/terms-and-conditions) on Wiley Online Library for rules of use; OA articles are governed by the applicable Creative Commons License

[46] P. Oliveri, C. Malegori, M. Casale, E. Tartacca, G. Salvatori, *Talanta* **2019**, *199*, 270.
[47] V. M. Corman, O. Landt, M. Kaiser, R. Molenkamp, A. Meijer, D. K. Chu, T. Bleicker, S. Brünink, J. Schneider, M. L. Schmidt, D. G. Mulders, B. L. Haagmans, B. van der Veer, S. van den Brink, L. Wijsman, G. Goderski, J.-L. Romette, J. Ellis, M. Zambon, M. Peiris, H. Goossens, C. Reusken, M. P. Koopmans, C. Drosten, *Eurosurveillance* **2020**, *25*, 2000045.
[48] L. Sarcina, F. Viola, F. Modena, R. A. Picca, P. Bollella, C. Di Franco, N. Cioffi, M. Caironi, R. Österbacka, I. Esposito, G. Scamarcio, L. Torsi, F. Torricelli, E. Macchia, *Anal. Bioanal. Chem.* **2022**, *414*, 5657.
[49] R. Ehsani, F. Drabløs, *Cancer Inform.* **2020**, *19*, 1176935120965542.
[50] E. Macchia, F. Giordano, M. Magliulo, G. Palazzo, L. Torsi, *Appl. Phys. Lett.* **2013**, *103*, 103301.
[51] R. Leardi, C. Melzi, G. Polotti, *CAT*, http://gruppochemiometria.it/index.php/software.

© 2025 The Author(s). Advanced Electronic Materials published by Wiley-VCH GmbH

2199160x, 0, Downloaded from https://onlinelibrary.wiley.com/doi/10.1002/aelm.202400908 by University Degli Studi Di Bari, Wiley Online Library on [04/02/2025]. See the Terms and Conditions (https://onlinelibrary.wiley.com/terms-and-conditions) on Wiley Online Library for rules of use; OA articles are governed by the applicable Creative Commons License